energies

MDPI

Article

Simulation-Based Parametric Sensitivity Analysis of a Natural Gas Combined-Cycle Plant with Amine-Based Post-Combustion CO_2 Capture

Abdul Rehman [1], Haris Khan [2,*], Ahmed Usman Yasir [1], Mirza Abdullah Rehan [3,*], Adnan Ibrahim [4,*], Muhammad Arslan [5], Muhammad Zubair Farrukh [6] and Sullah ud din [1]

[1] Department of Mechanical Engineering, Faculty of Mechanical and Aeronautical Engineering, University of Engineering and Technology (UET), Taxila 47080, Pakistan
[2] Department of Mechanical Engineering, Universiti Teknologi PETRONAS, Bandar Seri Iskandar 32610, Perak, Darul Ridzuan, Malaysia
[3] Department of Thermal Science and Energy Engineering, University of Science and Technology of China, Hefei 230027, China
[4] State Key Laboratory of Subtropical Building and Urban Science, South China University of Technology, Guangzhou 510641, China
[5] Department of Mechanical and Mechatronics Engineering, Memorial University of Newfoundland, St. John's, NL A1B 3X5, Canada
[6] Mechanical and Nuclear Engineering Department, Tennessee Technological University, Cookeville, TN 38505, USA; zubairfarrukh22@gmail.com
* Correspondence: haris22009966@utp.edu.my (H.K.); mierzaabdullah111@ustc.edu.cn (M.A.R.); adnanibrahim36@gmail.com (A.I.)

Abstract

Integrating post-combustion CO_2 capture (PCC) with natural gas combined-cycle (NGCC) power generation requires consideration of both power-cycle performance and capture-process requirements. This study develops an Aspen HYSYS model comprising two gas turbines, a heat recovery steam generator (HRSG), a steam turbine, and an amine-based CO_2 absorption–regeneration system. A one-variable-at-a-time sensitivity analysis examines the effects of compressor-stream temperature, pressure, and mass flow rate on individual turbine power outputs. Separate capture-process scans examine solvent circulation rate, absorber configuration and temperature, and regeneration conditions. These simulations identify individual parameter sensitivities but do not quantify interactions among the varied inputs or establish optimal plant operating conditions. Increasing the process-stream temperature from 100 to 500 °C raises the combined turbine outputs by 29.60 MW, while an analytical first-law assessment estimates an additional sensible-heating requirement of approximately 1206.0 MW using an air-equivalent specific heat approximation. These findings highlight the importance of accounting for thermal-energy requirements when evaluating turbine performance and overall plant efficiency. Increasing the mass flow rate from 500 to 5000 kg/s increases the first gas turbine output from 74.35 to 742.2 MW. A plant-wide assessment further accounts for auxiliary electrical consumption, steam extraction for solvent regeneration, and CO_2 compression requirements. The calculated net electrical output decreases from 547.73 MW without PCC to 465.74 MW with PCC, corresponding to a reduction in net thermal efficiency from 44.80% to 38.10%. At a CO_2 capture fraction of 90% and a specific reboiler duty of 3.80 GJ/t CO_2, direct CO_2 emissions intensity decreases from 459.44 to 54.03 kg CO_2/MWh. The results identify key operating parameters influencing power generation and CO_2 capture performance. The imposed temperature range is intended for model sensitivity analysis rather than

Academic Editors: Xinyuan Gao, Yiqi Zhang and Bin Shen

Received: 30 September 2026
Revised: 9 November 2026
Accepted: 13 November 2026
Published: 16 November 2026

Copyright: © 2026 by the authors. Licensee MDPI, Basel, Switzerland. This article is an open access article distributed under the terms and conditions of the Creative Commons Attribution (CC BY) license.

representing practical compressor-inlet conditions. These findings highlight the trade-off between CO_2 emissions reduction and the associated energy penalty in the integrated NGCC–PCC system.

Keywords: ASPEN HYSYS; CO_2 capture; steam turbine; gas turbine; power plants; emission reduction

1. Introduction

Rising global energy demand and continued dependence on fossil fuels have intensified the need to reduce greenhouse gas (GHG) emissions while maintaining reliable and efficient electricity generation [1,2]. Among conventional power-generation technologies, the Brayton and Rankine cycles are widely used, with the former typically employed in open-cycle gas turbines and the latter in closed-loop steam power systems. Integrating these two cycles in a combined-cycle power plant (CCPP) enables recovery of gas-turbine exhaust heat for steam generation, thereby improving overall thermal efficiency. Although renewable technologies such as solar and wind power offer low-carbon alternatives, their intermittency, relatively high capital costs, and energy-storage requirements can limit large-scale continuous power generation. In this context, the organic Rankine cycle (ORC) has attracted increasing attention because it uses low-boiling-point organic working fluids, enabling efficient conversion of low- and medium-temperature heat sources into electricity, with advantages including relatively simple operation, low maintenance requirements, and broad applicability to waste-heat recovery and renewable-energy systems [3,4]. Integrating amine-based post-combustion CO_2 capture (PCC) into thermal power plants offers a practical pathway for reducing CO_2 emissions from existing fossil-fuel-based generation, although the associated solvent regeneration energy demand and resulting efficiency penalty remain key challenges [5].

Recent studies have extensively investigated the thermodynamic performance, process integration, and CO_2 management in various power-generation systems, including natural gas combined-cycle (NGCC) power plants integrated with post-combustion capture (PCC) [6–9]. Canepa et al. developed a model for post-combustion CO_2 capture and proposed exhaust gas recirculation (EGR) to increase the CO_2 concentration in the flue gas while reducing its flow rate, thereby mitigating the thermal-efficiency penalty with minimal modification to the existing power plant [10]. Gu et al. performed a comprehensive analysis of an ORC integrated with a natural gas combined-cycle plant using Aspen HYSYS, evaluating ammonia-based working fluids at different concentrations. Their results showed that R-113 increased net power generation by 2.48% and overall energy efficiency by 6.2%, while reducing the cost of electricity by 10.75% [11]. Another effort by Biliyok et al. investigated CO_2 capture through process simulations and demonstrated that higher CO_2 concentrations in the exhaust gas enhance mass transfer; however, their economic analysis indicated that the integrated capture system increased the overnight plant cost by 58% compared with the reference power plant [12]. In another study, Taguchi-based design of experiments was applied to optimize post-combustion CO_2 capture from natural-gas-fired power plants using Aspen Plus. The analysis indicated that most operating parameters significantly affected the capture performance, whereas flue-gas temperature showed no statistically significant effect [13].

Baghsheikhi et al. conducted a 4E (energy, exergy, economic, and environmental) analysis of a combined-cycle power plant, considering both the environmental impacts of fossil-fuel-based generation and CO_2 capture from exhaust gases. The results indicated that lower ambient temperatures can improve the overall system efficiency [14]. Ahn et

al. compared different CO_2 capture technologies for combined-cycle power plants and evaluated their effects on net cycle performance and specific CO_2 capture. Their analysis identified an optimum pressure ratio for the oxy-combustion system, while the post-combustion capture configuration exhibited the highest efficiency but lower net power output [15]. Hu et al. developed an integrated NGCC system for simultaneous power generation and CO_2 capture using Honeywell UniSim Design, demonstrating increased power output compared with a conventional decarbonized NGCC configuration [16]. Similarly, Esquivel-Patiño et al. examined four CO_2 capture and utilization processes for the production of syngas, formic acid, and methanol and assessed thermal integration strategies to improve their energy, economic, and environmental performance. Strategic integration of hot and cold process streams was shown to improve energy efficiency and reduce energy demand by approximately 20–50% compared with the original capture and utilization configurations [17]. Li et al. investigated CO_2 capture integrated with soil thermal desorption and reported that irreversibilities associated with methane combustion and heat transfer limit exergy efficiency, while integrating CO_2 capture can substantially reduce emissions [18].

Amine-based PCC has received particular attention because of its established applicability to CO_2 capture, with recent pilot-scale investigations examining process performance and optimization [19]. A comparative study of five amine solvents demonstrated that CO_2 removal efficiency, energy consumption, solvent durability, and operational constraints must be considered simultaneously when selecting an appropriate solvent [20]. Adu et al. investigated the parametric design of large-scale amine-based PCC for both coal-fired and NGCC plants, using monoethanolamine (MEA) as the baseline solvent and evaluating the associated energy and economic performance [21]. Simulation studies have further shown that capture-process configuration and heat-recovery strategies can substantially influence regeneration energy consumption and net power generation [22]. Waste-heat recovery systems incorporating topping and bottoming cycles with indirect evaporative cooling have also been investigated to improve thermodynamic and techno-economic performance [23].

Process integration and heat recovery have emerged as important approaches for mitigating the efficiency penalty of PCC. Luo et al. [24] investigated NGCC integrated with PCC and exhaust gas recirculation (EGR), reporting substantial reductions in absorber and stripper size and changes in net plant efficiency. Kopac and Demirel examined the influence of thermodynamic and kinetic models on CO_2 capture performance using amine-based solvents [25]. Recent studies have also investigated dynamic optimization using water-lean solvents, ORC-based waste-heat recovery, CO_2 utilization pathways, and solar-assisted capture configurations [26–29]. Ali et al. investigated four configurations of an amine-based CO_2 capture system using a 30 wt.% aqueous MEA solution and a 90% CO_2 capture rate. Their study considered a natural-gas-fired combined-cycle system with a gross power output of 650 MWe and demonstrated that EGR could reduce the energy and cost penalties associated with CO_2 capture [30]. Liang et al. investigated the integration of CO_2 capture with waste-heat recovery and demonstrated that this approach reduced CO_2 regeneration energy consumption by 18.03% and increased net power efficiency from 48.88% to 50.10% [31]. Amrollahi et al. performed a thermodynamic and exergy analysis of an NGCC power plant integrated with MEA-based post-combustion CO_2 capture, identifying thermodynamic irreversibilities and opportunities for improved process integration [32]. Recent research has also explored multifunctional solid adsorbents for simultaneous carbon capture and mercury removal. Cheng et al. [33] investigated the synergistic adsorption of CO_2 and elemental mercury (Hg^0) through experiments and density functional theory calculations. Their work illustrates the application of combined experimental and molecular-level analysis to understand adsorption mechanisms in

emerging capture materials. Although this solid-adsorbent approach differs from the aqueous amine absorption process considered here, it broadens the technological context for post-combustion CO_2 capture. Rehman et al. presented a performance analysis and optimization of a natural-gas-fired combined-cycle power plant integrated with a post-combustion carbon capture process. They evaluated methods to minimize thermal efficiency penalties and optimize operating variables to improve net power generation [34].

Previous studies have investigated solvent selection, capture-process configuration, heat integration, and the energy and economic performance of NGCC plants with post-combustion CO_2 capture. The present study provides a simulation-based examination of how selected operating variables affect component-level turbine outputs and capture-process behavior in an Aspen HYSYS model. Compressor-stream temperature, pressure, and mass flow rate are varied individually, while separate analyses examine selected absorption and regeneration parameters. The objective is to identify model sensitivities and complement the separate plant-wide assessment of NGCC operation with and without PCC. The study does not quantify interactions among the varied inputs or determine an optimal operating point.

Although Aspen Plus and Aspen HYSYS have been widely applied to model NGCC and PCC systems, many existing studies focus on specific capture configurations, solvent behavior, or advanced integration strategies rather than systematically distinguishing component-level parameter sensitivities from plant-wide performance. Therefore, a process-simulation-based assessment of both aspects can provide a clearer understanding of their respective contributions to system performance. Accordingly, the present study develops an Aspen HYSYS model of an NGCC plant integrated with amine-based post-combustion CO_2 capture and systematically investigates the effects of process-stream temperature, pressure, and mass flow rate on individual turbine outputs, while separately evaluating net power generation, thermal efficiency, and CO_2 emissions for configurations with and without PCC. Exergy analysis and economic evaluation are outside the present scope. Consequently, the analysis does not establish an economically optimal operating condition or demonstrate the practical techno-economic feasibility of the integrated system.

2. Methodology

The NGCC–PCC process was modeled in Aspen HYSYS using industrial operating data. The model included two gas turbines, a heat recovery steam generator (HRSG), a steam turbine, and an amine-based absorption–regeneration unit. The overall process configuration is shown in Figure 1. The hydrocarbon fuel mixture and air constituents were defined first. The Peng–Robinson equation of state was used for the hydrocarbon system. The Aspen HYSYS Acid-Gas Chemical Solvent package was used for CO_2 absorption and solvent regeneration.

Model-stream temperature, pressure, and mass flow rate were varied separately. The remaining specified inputs were held at the reference conditions of each sweep. These simulations characterized component-level numerical responses rather than input interactions or optimal operating conditions. Capture-process trends were compared qualitatively with published studies in Section 3.3. The specific reboiler duty was benchmarked quantitatively against published NGCC–MEA studies and independent pilot-plant measurements in Section 3.3.1. ChatGPT (OpenAI) v6 was used to assist with language editing and proofreading, with the final content reviewed and approved by the authors.

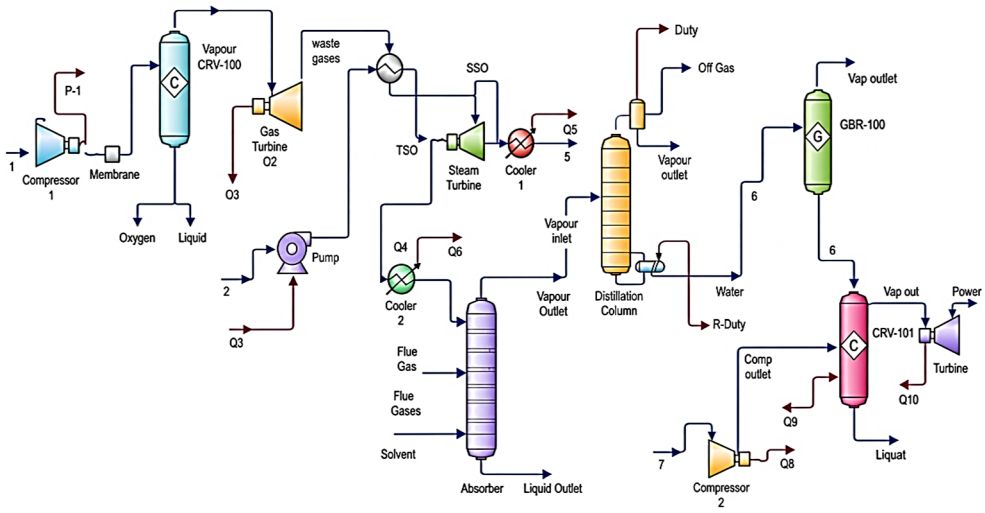


Figure 1. Aspen HYSYS flowsheet of the modeled NGCC plant with PCC. The system includes two gas turbines, an HRSG, a steam turbine, and an amine absorption–regeneration unit for CO_2 capture. Numbers identify process streams, while Q labels denote energy streams.

2.1. Process Simulation and Thermodynamic Framework

Aspen HYSYS V14.5 was used to model the NGCC plant with amine-based PCC. The natural-gas mixture contained methane, ethane, propane, n-butane, and n-pentane. The Peng–Robinson equation of state was applied to the hydrocarbon system. The PCC unit used the Aspen HYSYS Acid-Gas Chemical Solvent package, with a Peng–Robinson vapor phase and an electrolyte NRTL liquid phase with electrolyte reactions. A 30 wt.% aqueous monoethanolamine (MEA) solvent was used throughout. The absorber and stripper were modeled as equilibrium-stage columns rather than rate-based columns. The lean and rich loadings at the plant-wide reference condition were 0.25 and 0.48 mol CO_2/mol MEA, respectively. Reaction parameters were taken from the default HYSYS Acid-Gas library. The equilibrium-stage formulation does not resolve mass-transfer rates or packing height. Capture fraction in this model therefore depends on stage number, solvent circulation, and regeneration conditions. Model-stream temperature, pressure, and mass flow rate were selected for the component-level numerical sensitivity diagnostics. Capture-process behavior was assessed separately.

The imposed stream conditions in these diagnostics were distinct from the plant-wide reference case in Section 3.4.2. That case used a compressor-inlet temperature of 25 °C and a compressor pressure ratio of 20.02 to evaluate net electrical output and thermal efficiency under matched conditions. Quantitative predictions of MEA-based capture performance depend on vapor–liquid equilibrium, electrolyte speciation, reaction equilibria or kinetics, and solvent-regeneration enthalpy. These factors influence solvent CO_2 loadings, CO_2 removal efficiency, and reboiler duty. Thermodynamic and reaction models therefore require assessment against independent data. In this study, qualitative agreement in trends was distinguished from quantitative benchmarking. Agreement in the direction of a response alone was not treated as validation of reboiler-duty predictions.

2.2. Power Plant Configuration (Brayton and Rankine Cycle)

The modeled combined-cycle plant comprised two gas turbines and one steam turbine. The gas turbines operate on the Brayton cycle, whereas the steam turbine operates on the Rankine cycle. Compressed air is mixed with natural gas and combusted. The hot combustion gases expand through the gas turbines to produce power. Exhaust heat is recovered in the HRSG to generate steam for the steam turbine. This recovery improves efficiency by using heat that would otherwise be rejected.

Changes in upstream stream conditions affect turbine expansion, exhaust conditions, HRSG steam generation, and steam-turbine output. State 1 denotes the compressor inlet, state 2 the compressor outlet, state 3 the turbine inlet, and state 4 the turbine outlet. Compressor pressure ratio and component isentropic efficiencies determine compression and expansion work. The calculations assumed steady, approximately adiabatic operation and negligible changes in kinetic and potential energy. Work was evaluated from the corresponding stream enthalpies.

2.3. Post-Combustion Capture (PCC) and Solvent Regeneration

The post-combustion CO_2 (PCC) capture system is integrated downstream of the HRSG and consists of an absorber and a stripper for solvent regeneration. After cooling, the flue gas enters the absorber and contacts the amine-based solvent counter-currently, allowing CO_2 to be selectively absorbed and form a CO_2-rich solvent. The treated flue gas exits from the absorber, while the rich solvent is transferred to the stripper, where reboiler heat releases the absorbed CO_2 as a concentrated stream for subsequent storage or utilization. The regenerated lean solvent is recycled to the absorber, forming a continuous circulation loop. PCC performance is governed by key operating and design parameters, including solvent circulation rate, absorber temperature, number of stages, and reboiler temperature. These variables affect CO_2 capture efficiency and the energy demand of solvent regeneration, particularly the reboiler duty. Integration with the NGCC plant enables simultaneous assessment of power-generation performance. Reference capture-unit settings used for the plant-wide assessment include a 30 wt.% aqueous MEA solution, lean and rich CO_2 loadings of 0.25 and 0.48 mol CO_2/mol MEA, respectively, 15 equilibrium stages in the absorber, 10 equilibrium stages in the stripper, and a reboiler temperature of 120 °C. Under these conditions, the Aspen HYSYS model predicts a specific reboiler duty of 3.80 GJ/t CO_2, which is quantitatively compared with published NGCC–MEA results in Section 3.3.1.

2.4. Plant-Wide Power Balance and Performance Definitions

A complete plant-wide assessment must distinguish turbine power generation from net electrical output. Net plant output requires accounting for compressor consumption, mechanical and generator losses where applicable, and auxiliary electricity demands. These auxiliary demands include feedwater pumps, solvent circulation pumps, cooling equipment, flue-gas handling, and CO_2 compression. Compressor consumption must be deducted only when it is not already included in the reported gas-turbine output.

Solvent regeneration also affects plant performance through the steam required to supply the reboiler. Quantifying this effect requires coupling reboiler duty to steam-extraction conditions, condensate return, and the resulting reduction in steam-turbine generation. When this reduction is already included in the calculated steam-turbine output, it must not be deducted again. Reboiler duty must be reported separately from electrical consumption.

Net electrical efficiency is defined as net electrical output divided by fuel-energy input on a consistent lower-heating-value basis. Capture-related power and efficiency penalties must be determined by comparing cases with and without capture under matched fuel-input and operating conditions.

Compressor consumption and auxiliary loads were included in the plant-wide energy balance in Section 3.4. The reduction in steam-turbine output due to solvent regeneration was also included. The component-level sensitivity results represent individual turbine outputs rather than net plant electrical output. The plant-wide assessment presents net electrical output and thermal efficiency for configurations with and without PCC

at the same fuel-energy input. Reboiler duty was reported separately from electrical consumption to avoid double counting.

2.5. Parametric Sensitivity Analysis

A one-variable-at-a-time analysis was performed by varying model-stream temperature, pressure, and mass flow rate separately. The remaining specified inputs were held at the reference conditions of each sweep. Outputs from both gas turbines and the steam turbine were recorded. Separate scans examined solvent circulation rate, absorber conditions, and regeneration conditions. Each scan characterized the response to one input under its specified references. Connected process units responded to each perturbation, but the analysis did not quantify interactions caused by simultaneous changes in multiple inputs. No objective function or constrained optimization algorithm was used. The results were therefore interpreted as component-level numerical sensitivity diagnostics rather than optimized operating conditions.

The temperature and pressure ranges represented numerical perturbations of model-stream conditions. They were not practical compressor operating ranges. The plant-wide reference calculation in Section 3.4.2 used a compressor-inlet temperature of 25 °C and a pressure ratio of 20.02. It did not provide a separate sensitivity analysis over realistic compressor conditions.

Temperatures in the diagnostic sweep were specified boundary conditions rather than outputs of a modeled heating system. Their sensible-heating requirements were estimated analytically in Analytical Energy Assessment of the Temperature Sensitivity (Section 3.2) using a constant air-equivalent specific heat. For a nonreacting stream heated at constant pressure and composition, the general thermal-energy requirement is expressed as

$$\dot{\boldsymbol{Q}}_{\text{heat}} = \dot{\boldsymbol{m}}\left[\boldsymbol{h}\left(\boldsymbol{T}_{\text{specified}}, \boldsymbol{p}, \mathbf{x}\right) - \boldsymbol{h}\left(\boldsymbol{T}_{\text{reference}}, \boldsymbol{p}, \mathbf{x}\right)\right]$$

where $\dot{\boldsymbol{Q}}_{\text{heat}}$ is the heating rate (kW), $\dot{\boldsymbol{m}}$ is the stream mass flow rate (kg s^{-1}), $\boldsymbol{h}$ is the specific enthalpy (kJ kg^{-1}), $\boldsymbol{T}$ is the absolute temperature (K), $\boldsymbol{p}$ is the stream pressure (Pa), and $\mathbf{x}$ denotes the dimensionless stream-composition vector. If pressure changes involve compression, the corresponding compressor work must also be considered. Consequently, the reported increases in individual turbine outputs do not independently establish improvements in net electrical output or thermal efficiency. A complete plant-wide assessment would additionally consider the heating source, fuel consumption, auxiliary loads, and associated heat-recovery effects.

3. Results and Discussion

3.1. Component-Level Numerical Sensitivity Diagnostics for Temperature and Pressure

Table 1 summarizes the ranges used in the component-level numerical sensitivity diagnostics. The specified compressor stream contained a representative mixture of natural-gas and air constituents: methane, ethane, propane, n-butane, n-pentane, nitrogen, and oxygen. The imposed temperature range was 100–500 °C, the pressure range was 60–105 bar, and the mass-flow range was 500–5000 kg/s. These broad stream-state ranges were used for numerical diagnostics rather than to represent practical compressor-inlet conditions. The plant-wide assessment in Section 3.4 used a compressor-inlet temperature of 25 °C and a pressure ratio of 20.02. That matched-case comparison of operation with and without PCC did not validate or extend the imposed high-temperature diagnostic results.

Sections 3.1 and 3.2 present component-level numerical sensitivity diagnostics. Each sweep used different fixed references: 60 bar and 3000 kg/s for temperature; 1273 °C and 96.98 kg/s for pressure; and 270 °C and 60 bar for mass flow. Output magnitudes and slopes must not be ranked across the three sweeps or interpreted as comparable

sensitivities about a common operating point. These diagnostics do not establish practical compressor-inlet behavior or operating recommendations. Table 2 reports the turbine responses to the imposed model-stream temperature sweep from 100 to 500 °C. Predicted output increased from 1.9 to 12.7 MW for Gas Turbine 1, from 0.7 to 10.8 MW for the steam turbine, and from 0.3 to 9.0 MW for Gas Turbine 2. These increases occurred within the imposed thermal boundary, which supplied additional sensible energy to the model stream. The values represent component outputs rather than net plant electrical output. Their interpretation is valid only within this heating boundary and must not be extrapolated to practical compressor-inlet conditions. Heating compressor-inlet air reduces its density. An increase in component output without accounting for the external heat input does not demonstrate improved net plant efficiency. Analytical Energy Assessment of the Temperature Sensitivity (Section 3.2) quantifies the associated sensible-heating requirement; it does not establish a practical inlet-heating benefit.

Table 1. Imposed model-stream ranges and nominal settings used for the component-level numerical diagnostics.

Component	Working Fluid	Temperature Range (°C)	Pressure Range (bar)	Mass Flow Rate Range (kg/s)	Nominal Value		
					Temperature (°C)	Pressure (bar)	Mass Flow Rate (kg/s)
Compressor	Oxygen, Methane, Ethane, Propane, Nitrogen, n-butane, n-pentane	100–500	60–105	500–5000	270	60	3000

Table 2. Individual turbine outputs (MW) for imposed model-stream temperatures of 100–500 °C at 60 bar and 3000 kg/s.

Compressor Temperature (°C)	Gas Turbine 1 (MW)	Steam Turbine (MW)	Gas Turbine 2 (MW)
100	1.9	0.7	0.3
200	3.9	2.0	1.3
300	6.8	4.3	3.0
400	10.3	7.6	5.7
500	12.7	10.8	9.0

Table 3 presents the component-level response to model-stream pressure varied from 60 to 105 bar at fixed reference conditions of 1273 °C and 96.98 kg/s. These pressures refer to the specified HYSYS process stream and should not be interpreted as actual compressor-inlet pressures or compressor pressure ratios. Gas Turbine 1 output decreases from 5.994 MW at 60 bar to 3.00 MW at 105 bar (Table 3). Similarly, steam-turbine output decreases from 1.775 to 0.390 MW, while Gas Turbine 2 output declines from 1.200 to 0.248 MW across the investigated pressure range. Thus, all three turbines exhibit a consistent decrease in power output with increasing pressure. These results alone do not establish an optimal operating pressure; determining an optimum requires a clearly defined performance objective, such as maximum net power or thermal efficiency, together with compressor power consumption and relevant operating constraints.

Table 3. Individual turbine outputs (MW) for imposed model-stream pressures of 60–105 bar at 1273 °C and 96.98 kg/s.

Compressor Pressure (bar)	Gas Turbine 1 (MW)	Steam Turbine (MW)	Gas Turbine 2 (MW)
60	5.994	1.775	1.20
65	4.978	1.071	0.835
70	4.317	0.778	0.723
75	3.829	0.614	0.551
80	3.449	0.509	0.415
85	3.142	0.435	0.388
90	3.116	0.429	0.349
95	3.100	0.415	0.325
100	3.055	0.392	0.254
105	3.00	0.39	0.248

3.2. Component-Level Numerical Sensitivity Diagnostics for Mass Flow Rate

Figure 2 reports the component-level numerical response to model-stream mass flow at fixed reference conditions of 270 °C and 60 bar. Increasing mass flow from 500 to 5000 kg/s raised Gas Turbine 1 output from 74.35 to 742.2 MW. Steam-turbine output increased from 10.25 to 102.3 MW, and Gas Turbine 2 output increased from 7.32 to 92.987 MW. These increases reflected greater working-fluid throughput and associated energy flow under the imposed simulation conditions. The higher exhaust-gas flow also increased heat availability to the HRSG, supporting greater steam generation and steam-turbine output.

These results describe the throughput response within this diagnostic only. Their magnitudes must not be ranked against those of the temperature and pressure sweeps because the fixed reference conditions differ. Increased component output does not establish improved efficiency or optimal plant capacity; compressor consumption, fuel input, capture energy requirements, and equipment constraints must also be evaluated. The highest component output within a scan therefore represents only the highest reported value under that scan's imposed conditions.

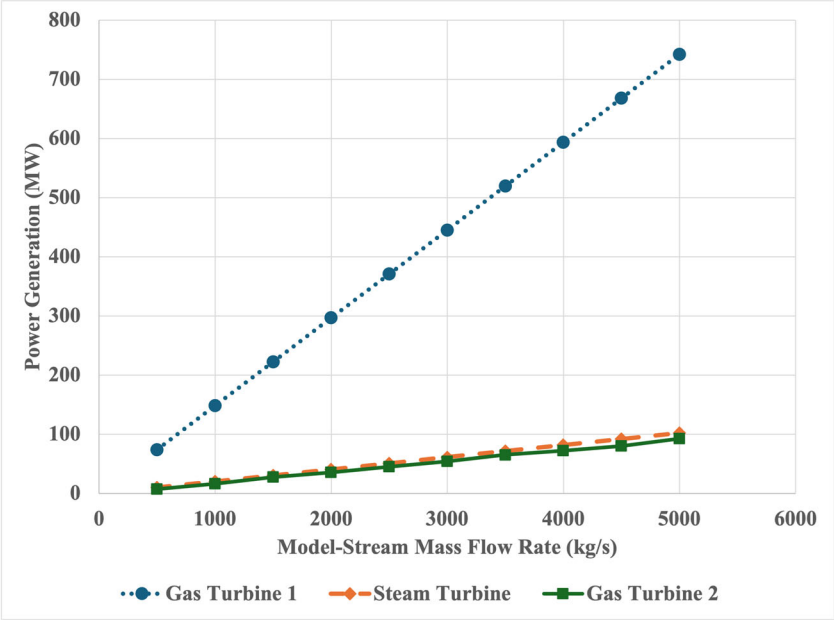


Figure 2. Variation in individual turbine power outputs with model-stream mass flow rate at 270 °C and 60 bar [34].

Table 4 summarizes selected simulation conditions and the corresponding turbine outputs. The reported outputs increase across the selected cases as temperature, pressure, and mass flow rate vary simultaneously. These changes cannot be attributed to temperature alone. Pressure affects the working-fluid state and compression and expansion requirements, while mass flow affects energy throughput and exhaust-heat availability. The imposed temperature conditions also involve sensible-heating requirements, as assessed for the separate temperature sweep in Analytical Energy Assessment of the Temperature Sensitivity (below). Because multiple inputs change between successive cases, these results illustrate combined numerical responses rather than isolated parameter sensitivities, optimized operating conditions, or improvements in net plant efficiency.

Table 4. Selected imposed model-stream conditions and turbine outputs. Temperature, pressure, mass flow, and output are reported in °C, bar, kg/s, and MW.

Compressor Temperature (°C)	Compressor Pressure (bar)	Compressor Mass Flow Rate (kg/s)	Gas Turbine 1 (MW)	Steam Turbine (MW)	Gas Turbine 2 (MW)
100	60	500	35.24	33.68	25.22
200	65	600	47.47	44.12	33.59
300	70	700	54.92	51.30	40.73
400	75	800	61.74	55.21	48.89
500	80	1000	65.08	60.73	52.76

Figure 3 shows component-level numerical responses to the imposed model-stream temperature at fixed reference conditions of 60 bar and 3000 kg/s. The increase in turbine output is attributable to the imposed thermal boundary and its added sensible energy. It does not demonstrate that higher practical compressor-inlet temperature improves gas-turbine performance. These results are valid only within this boundary and must not be extrapolated to practical compressor-inlet conditions, where heating reduces air density.

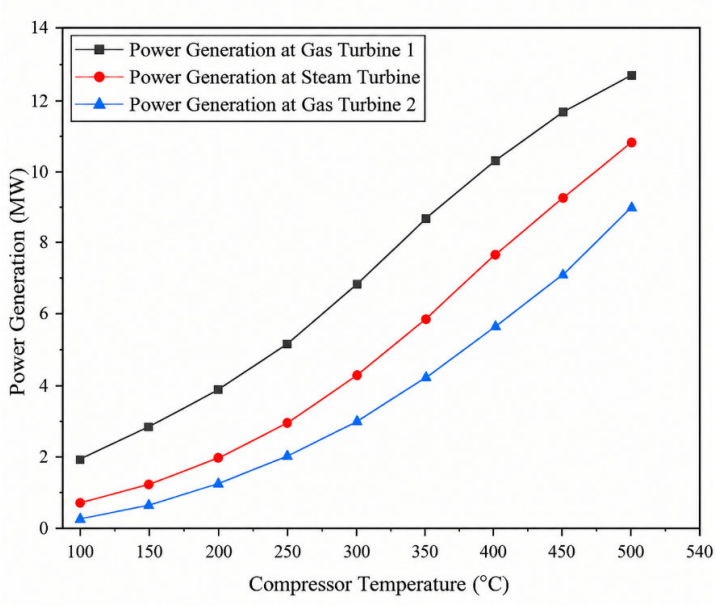


Figure 3. Component-level numerical response to imposed model-stream temperature at 60 bar and 3000 kg/s.

Analytical Energy Assessment of the Temperature Sensitivity

To evaluate the thermal-energy implications of the imposed temperature sweep, a first-law assessment was conducted using the operating conditions in Table 2. The analysis considers a model-stream mass flow rate of 3000 kg/s at a constant pressure of 60 bar. The sensible-heating requirement was estimated relative to 25 °C using an air-equivalent specific heat of 1.005 kJ/(kg·K), consistent with the representative air-property approximation in Section 3.4.2. Pressure and stream composition were held constant.

The corresponding sensible-heating requirement is given by

$$\dot{\boldsymbol{Q}}_{\mathrm{h}} = \frac{\dot{\boldsymbol{m}}_{\mathrm{s}}\, \boldsymbol{c}_{\mathrm{p}}\, (\boldsymbol{T} - \boldsymbol{T}_{\mathrm{ref}})}{\mathbf{1000}}\ \mathrm{MW}$$

where $\dot{\boldsymbol{Q}}_{\mathrm{h}}$ is the sensible-heating requirement (MW), $\dot{\boldsymbol{m}}_{\mathrm{s}}$ is stream mass flow rate (kg/s), $\boldsymbol{c}_{\mathrm{p}}$ is specific heat capacity (kJ/(kg·K)), $\boldsymbol{T}$ is the imposed stream temperature (°C), and $\boldsymbol{T}_{\mathrm{ref}}$ is the reference temperature (25 °C). Temperature differences are evaluated in kelvin, and division by 1000 converts kJ/s to MW. The estimated sensible-heating requirements and corresponding combined turbine outputs are summarized in Table 5.

Table 5. Estimated sensible-heating requirements and combined turbine outputs for the temperature diagnostic at 60 bar and 3000 kg/s. Heating is referenced to 25 °C using an air-equivalent specific heat of 1.005 kJ/(kg·K).

Temperature (°C)	Combined Turbine Output (MW)	Sensible Heating from 25 °C (MW Thermal)	Additional Heating Relative to 100 °C (MW Thermal)	Turbine-Output Gain Relative to 100 °C (MW)
100	2.90	226.1	0.0	0.0
200	7.20	527.6	301.5	4.3
300	14.10	829.1	603.0	11.2
400	23.60	1130.6	904.5	20.7
500	32.50	1432.1	1206.0	29.6

From 100 to 500 °C, the additional sensible-heating requirement and the increase in combined reported turbine output are, respectively,

$$\Delta\dot{\boldsymbol{Q}}_{\mathrm{h}} = \frac{\mathbf{3000} \times \mathbf{1.005} \times (\mathbf{500} - \mathbf{100})}{\mathbf{1000}} = \mathbf{1206.0}\ \mathrm{MW}$$

$$\Delta\boldsymbol{P}_{\mathrm{turb}} = (\mathbf{12.7} + \mathbf{10.8} + \mathbf{9.0}) - (\mathbf{1.9} + \mathbf{0.7} + \mathbf{0.3}) = \mathbf{29.60}\ \mathrm{MW}$$

The incremental turbine-output-to-heating ratio was therefore

$$\boldsymbol{R}_{\mathrm{inc}} = \frac{\Delta\boldsymbol{P}_{\mathrm{turb}}}{\Delta\dot{\boldsymbol{Q}}_{\mathrm{h}}} \times \mathbf{100\%} = \frac{\mathbf{29.60}}{\mathbf{1206.0}} \times \mathbf{100\%} = \mathbf{2.45\%}$$

Increasing the imposed model-stream temperature from 100 to 500 °C raised the combined turbine outputs by 29.60 MW. The estimated additional sensible-heating requirement was 1206.0 MW. The incremental turbine-output-to-heating ratio was therefore 2.45%. This ratio compares the component-output increase with the estimated additional thermal input; it is not net plant thermal efficiency. At 270 °C and 3000 kg/s, the estimated sensible-heating requirement relative to 25 °C was 738.7 MW under the same assumptions. This assessment provides a thermodynamic basis for interpreting the temperature sensitivity results by accounting for the associated sensible-energy requirements. The plant-wide analysis in Section 3.4 separately evaluates net electrical output and thermal efficiency under matched reference conditions, incorporating compressor consumption, auxiliary loads, steam extraction, and CO_2 compression. Together, these analyses distinguish temperature-dependent turbine-output variations from the overall energy

performance of the integrated NGCC–PCC system while maintaining consistency with their respective operating conditions.

Figure 4 shows the turbine responses to imposed model-stream pressure at 1273 °C and 96.98 kg/s. Increasing pressure from 60 to 105 bar reduced Gas Turbine 1 output from approximately 6.0 to 3.0 MW. Steam-turbine output decreased from 1.775 to 0.390 MW, and Gas Turbine 2 output decreased from 1.200 to 0.248 MW. These results characterize the numerical response under the specified pressure-sweep references. They do not establish practical compressor-inlet behavior or an optimal pressure. Their magnitudes must not be ranked against the other sweeps, which used different fixed references.

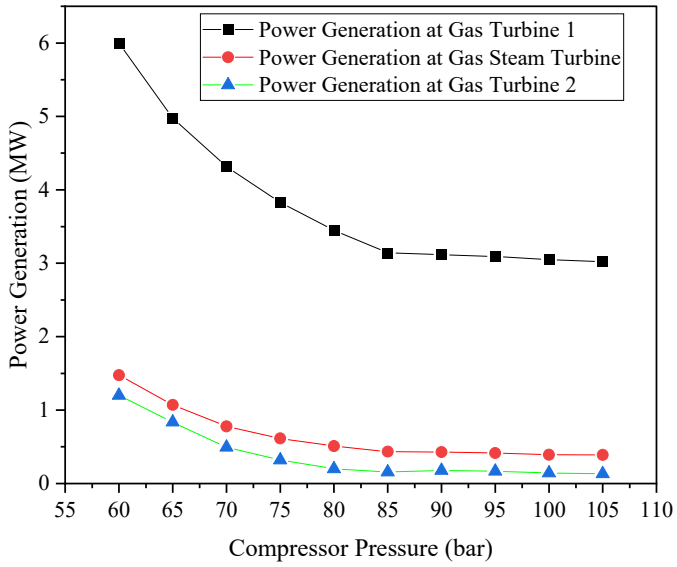


Figure 4. Individual turbine outputs (MW) versus imposed model-stream pressure (bar) at 1273 °C and 96.98 kg/s.

3.3. Post-Combustion CO_2 Capture Performance and Comparison with Literature

The MEA-based capture model was evaluated using parameter scans and comparisons with published studies. Figures 5–8 show the effects of solvent circulation rate, absorber stage number, absorber inlet-gas temperature, and reboiler temperature. The plotted outputs are CO_2 removal efficiency and specific reboiler duty.

Simulated trends were compared qualitatively with published aqueous-MEA results. The reference specific reboiler duty of 3.80 GJ/t CO_2 was benchmarked quantitatively against simulation and pilot-plant results in Section 3.3.1. Section 3.3.2 examines solvent mass-balance consistency and compares operating parameters with the NGCC–MEA case of Ali et al. [30]. Figure 5 shows that higher solvent circulation generally increased simulated CO_2 removal over the investigated range. The specific reboiler duty also increased at higher circulation rates. Greater solvent flow increases the amount of liquid requiring heating and regeneration. Selecting a circulation rate therefore requires balancing CO_2 removal against regeneration energy requirements. This scan did not establish an optimal circulation rate.

Figure 6 shows the response to absorber stage number. Simulated CO_2 removal increased as the number of equilibrium stages increased. The specific reboiler duty decreased over the plotted range. Additional equilibrium stages provide more modeled gas–liquid contacting steps. The formulation does not directly resolve the contact area, residence time, mass-transfer rates, or packing height. The results therefore do not quantify these physical mechanisms or determine equipment dimensions. Practical stage selection

also requires equipment and cost assessment. The magnitude of the predicted response requires quantitative validation.

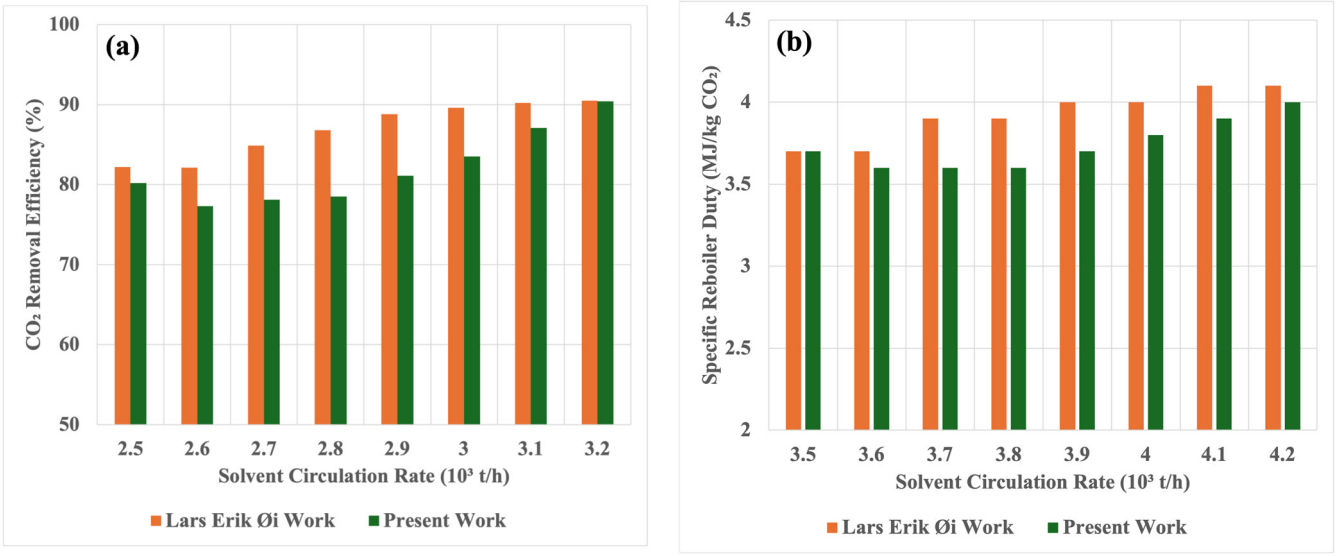


Figure 5. Comparison of (**a**) CO_2 removal efficiency (%) and (**b**) specific reboiler duty (MJ/kg CO_2) versus solvent circulation rate (10^3 t/h) for Lars Erik Øi's work and the present study [34].

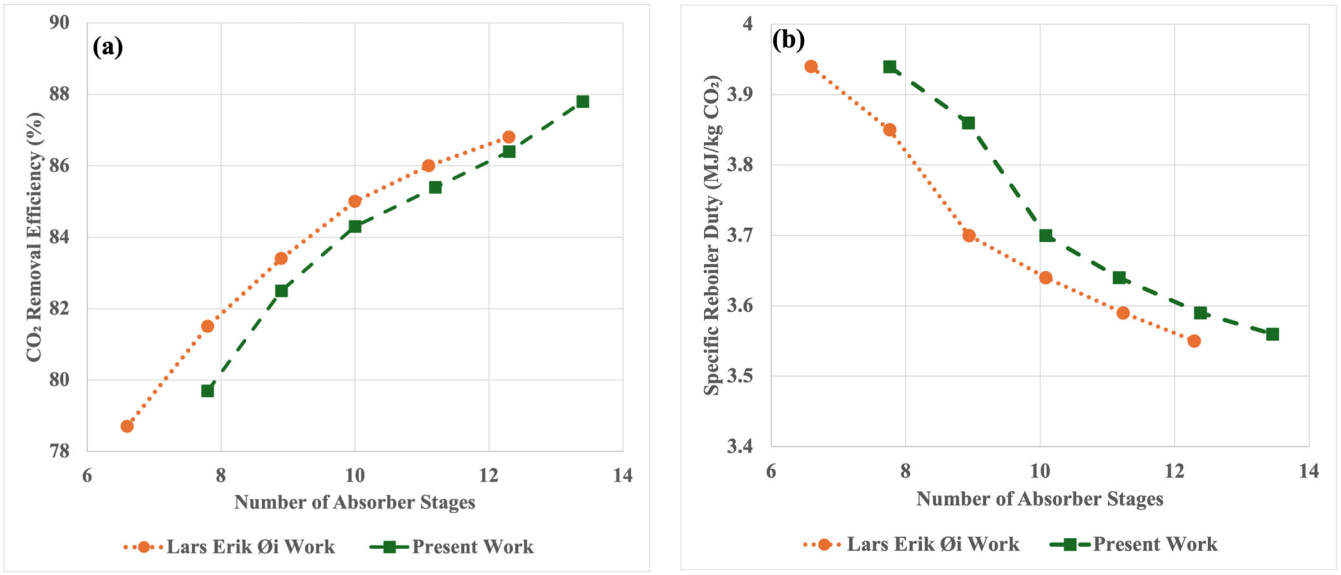


Figure 6. Comparison of (**a**) CO_2 removal efficiency (%) and (**b**) specific reboiler duty (MJ/kg CO_2) versus absorber stage number for Lars Erik Øi's work and the present study [34].

Figure 7 shows the response to absorber inlet-gas temperature. Increasing temperature from approximately 31 to 51 °C raised simulated CO_2 removal from 84.7% to 89.5%. The specific reboiler duty decreased from approximately 3.67 to 3.55 MJ/kg CO_2. Amine-based CO_2 absorption is generally exothermic, but the calculated removal increased over this scan. The response reflected the combined imposed conditions and equilibrium-stage model. The trend alone did not establish its underlying physical mechanism or quantitative prediction accuracy.

Figure 8 shows the response to reboiler temperature. Increasing temperature from 119 to 121 °C reduced the simulated specific reboiler duty from approximately 3.90 to 3.80 MJ/kg CO_2. CO_2 removal decreased slightly, from 85.07% to 85.01%. Thus, the lower

specific reboiler duty was not accompanied by improved removal. The scan did not establish an optimal temperature or quantify solvent degradation.

The plant-wide reference specific reboiler duty of 3.80 GJ/t CO_2 was obtained using the settings in Section 2.3. Benchmarking in Section 3.3.1 gave absolute differences of 0.78–7.99% relative to published NGCC–MEA values of 3.73–4.13 GJ/t CO_2. The difference relative to the independent NCCC pilot-plant measurement was approximately 9.52%. These comparisons supported agreement in the magnitude of the specific reboiler duty under the respective study conditions.

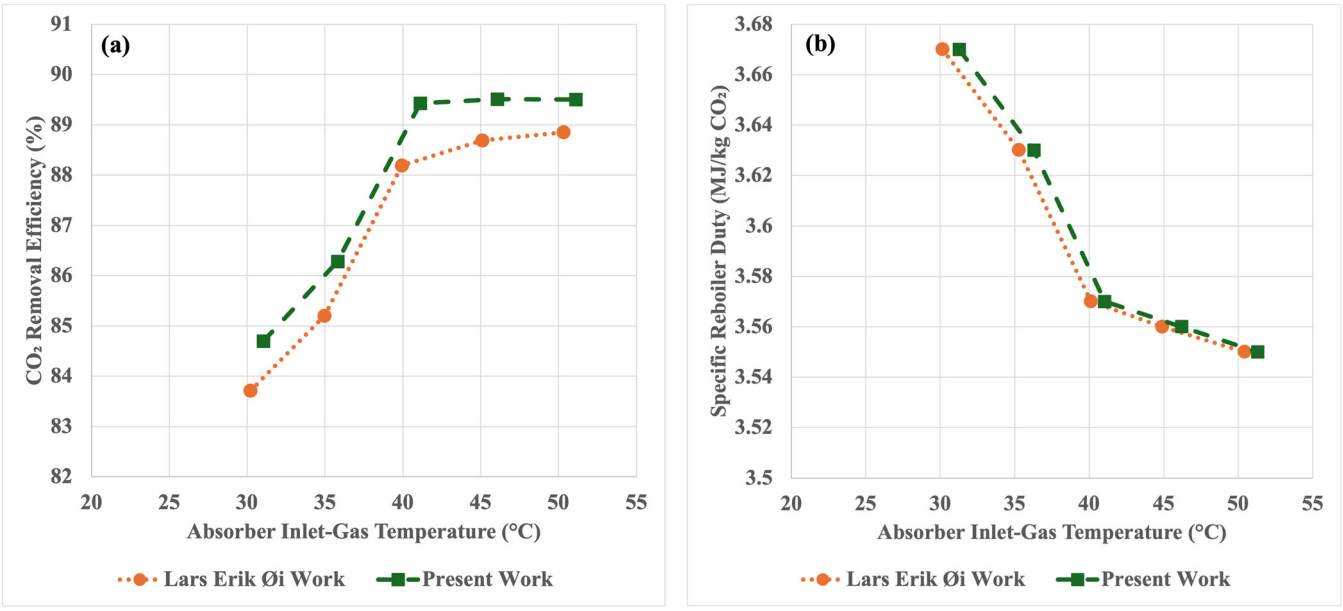


Figure 7. Comparison of (**a**) CO_2 removal efficiency (%) and (**b**) specific reboiler duty (MJ/kg CO_2) versus absorber inlet-gas temperature (°C) for Lars Erik Øi's work and the present study [34].

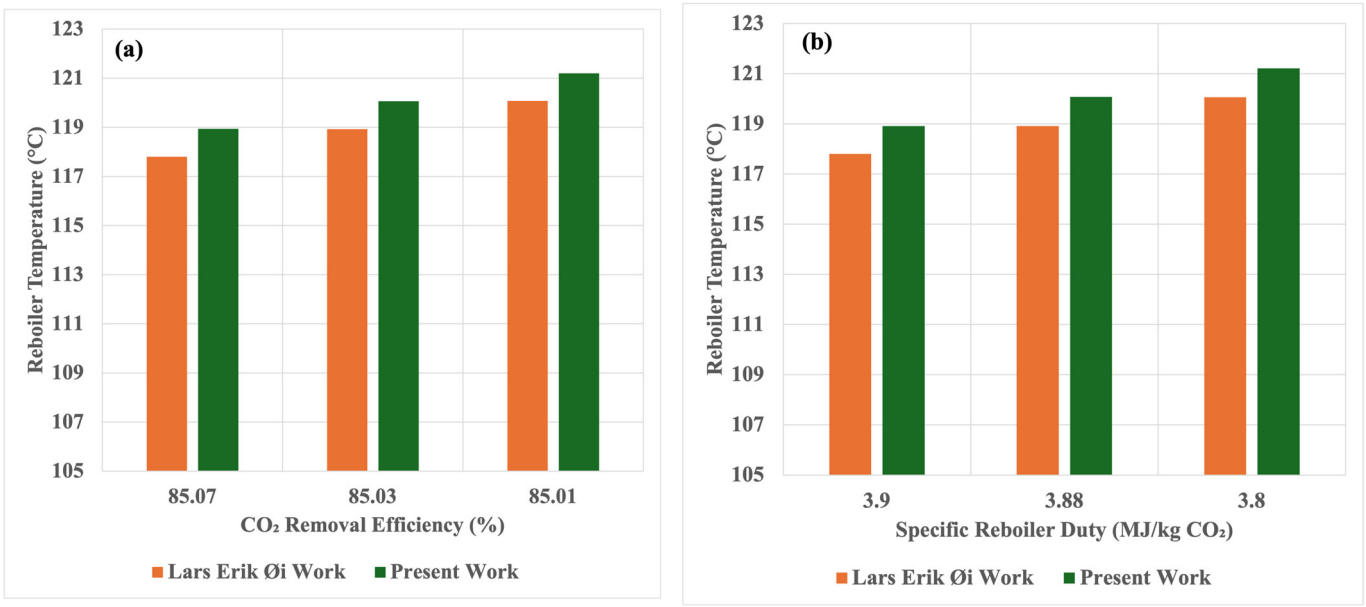


Figure 8. Comparison of reboiler temperature (°C) with (**a**) CO_2 removal efficiency (%) and (**b**) specific reboiler duty (MJ/kg CO_2) for Lars Erik Øi's work and the present study [34].

Table 6 summarizes selected findings from previous studies. Section 3.3.1 provides a quantitative comparison of specific reboiler duty with published NGCC–MEA

simulations and independent pilot-plant measurements. Absolute differences across the three NGCC simulation references were 0.78–7.99%, with a mean absolute percentage difference (MAPD) of 3.55%. The NCCC pilot result was assessed separately. Differences in flue-gas composition, solvent loading, and equipment configuration were considered when interpreting the comparisons. Further validation under matched conditions would strengthen the assessment of CO_2 removal, solvent loadings, and reboiler duty.

Table 6. Selected published studies relevant to NGCC generation, CO_2 capture, and process integration.

Study	Focus Area	Key Findings
Amrollahi et al. [32]	Exergy Analysis	21.2% increase in efficiency
Canepa et al. [10]	EGR Integration	EGR raises CO_2 concentration
Gu et al. [11]	ORC Coupling	Net power output increases by 2.48%
Biliyok et al. [12]	Economic	Integrated plant cost was 58% higher
Adu et al. [21]	Solvent Optimization	Up to 41.8% energy savings
Luo et al. [24]	Advanced Integration	Combined EGR and heat integration recovered efficiency to 50.47%
Present Study	Integrated Parametric Sensitivity Analysis	Evaluates turbine-output sensitivities, CO_2 capture behavior, and matched-case net plant performance

3.3.1. Quantitative Benchmarking of the MEA-Based CO_2 Capture System

The specific regeneration-energy requirement of the MEA-based post-combustion CO_2 capture system was compared with published NGCC capture studies and independent pilot-plant measurements. The present NGCC–PCC configuration employs $\mathbf{30\ wt\%}$ aqueous monoethanolamine (MEA), a $\mathbf{90\%}$ CO_2 capture fraction, and lean and rich solvent loadings of $\mathbf{0.25}$ and $\mathbf{0.48\ mol\ CO_2/mol\ MEA}$, respectively. The Aspen HYSYS reference case reports a reboiler heat duty of $\mathbf{239.07\ MW}$, a captured CO_2 mass flow rate of $\mathbf{62.91\ kg\ s^{-1}}$, and a specific reboiler duty of $\mathbf{3.80\ GJ\ t^{-1}\ CO_2}$.

The specific reboiler duty was obtained by normalizing the reported reboiler thermal load by the captured CO_2 mass flow rate:

$$\mathbf{q_{reb}} = \frac{\mathbf{\dot{Q}_{reb}}}{\mathbf{\dot{m}_{CO_2,cap}}} = \frac{\mathbf{239.07\ MW}}{\mathbf{62.91\ kg\ s^{-1}}} = \mathbf{3.80\ GJ\ t^{-1}\ CO_2}.$$

Reference values were selected from the no-exhaust-gas-recirculation NGCC case of Ali et al. [30], the standard NGCC–MEA case of Aromada et al. [35], and the optimized NGCC capture case of Adu et al. [1]. A baseline $\mathbf{30\ wt\%}$ MEA pilot measurement from the National Carbon Capture Center (NCCC) [36] provides an additional experimental comparator. The operating conditions differ among the studies; thus, the comparison evaluates the reported magnitude of the regeneration duty rather than a common-condition model prediction.

For each published case $\mathbf{i}$, the absolute percentage difference relative to the published duty is calculated as

$$\mathbf{d_i} = \mathbf{q_{present}} - \mathbf{q_{ref,i}};\quad \boldsymbol{\delta}_\mathbf{i} = \frac{\mathbf{100} \times \mathbf{abs(d_i)}}{\mathbf{q_{ref,i}}}\ (\%)$$

To summarize the comparisons, the mean absolute percentage difference (MAPD), mean squared difference (MSD), and root mean square difference (RMSD) are defined as

$$\mathbf{MAPD} = \frac{\mathbf{1}}{\mathbf{n}}\ \mathbf{\Sigma}\ \boldsymbol{\delta}_\mathbf{i} = \mathbf{3.55\%};$$

$$\mathbf{MSD} = \frac{\mathbf{1}}{\mathbf{n}} \Sigma (\mathbf{q_{present}} - \mathbf{q_{ref,i}})^2 = \mathbf{0.0382\ (GJ\ t^{-1}\ CO_2)^2};$$

$$\mathbf{RMSD} = \sqrt{(\mathbf{MSD})} = \mathbf{0.196\ GJ\ t^{-1}\ CO_2}.$$

Table 7 shows that the present specific reboiler duty of 3.80 GJ t^{-1} CO_2 lies within the 3.73–4.13 GJ t^{-1} CO_2 range reported in the three published NGCC–MEA simulations. The absolute percentage differences are 0.78% relative to Ali et al. [30], 1.88% relative to Aromada et al. [35], and 7.99% relative to Adu et al. [1]. The independent NCCC pilot result of approximately 4.20 GJ t^{-1} CO_2 corresponds to a 9.52% difference. As summarized in Table 8, across the three simulation cases, the MAPD is 3.55%, the MSD is 0.0382 (GJ t^{-1} CO_2)^2, and the RMSD is 0.196 GJ t^{-1} CO_2. Figure 9 provides a visual comparison of the specific reboiler duties.

Table 7. Specific reboiler duty (GJ/t CO_2), feed CO_2 concentration, lean solvent loading, and absolute percentage differences for the present case and published reference cases.

Study	Reboiler Duty (GJ t^{-1} CO_2)	Feed CO_2 (mol%)	Lean Loading (mol/mol)	Absolute Difference (%)
Present study	3.80	4.08 (wet)	0.25	—
Ali et al. (2016) [30]	3.83	3.91	0.20	0.78
Aromada et al. (2022) [35]	3.73	3.75	0.26	1.88
Adu et al. (2020) [1]	4.13	4.04	0.2307	7.99
NCCC pilot (2022) [36]	4.20	≈ 4.41	—	9.52

Table 8. Descriptive differences between the present specific reboiler duty and the three published NGCC–MEA simulation references.

Statistic	Calculated Value	Interpretation
Mean absolute percentage difference (MAPD)	3.55%	Percentage
Mean squared difference (MSD)	0.0382 (GJ t^{-1} CO_2)^2	Squared duty
Root mean square difference (RMSD)	0.196 GJ t^{-1} CO_2	Specific duty

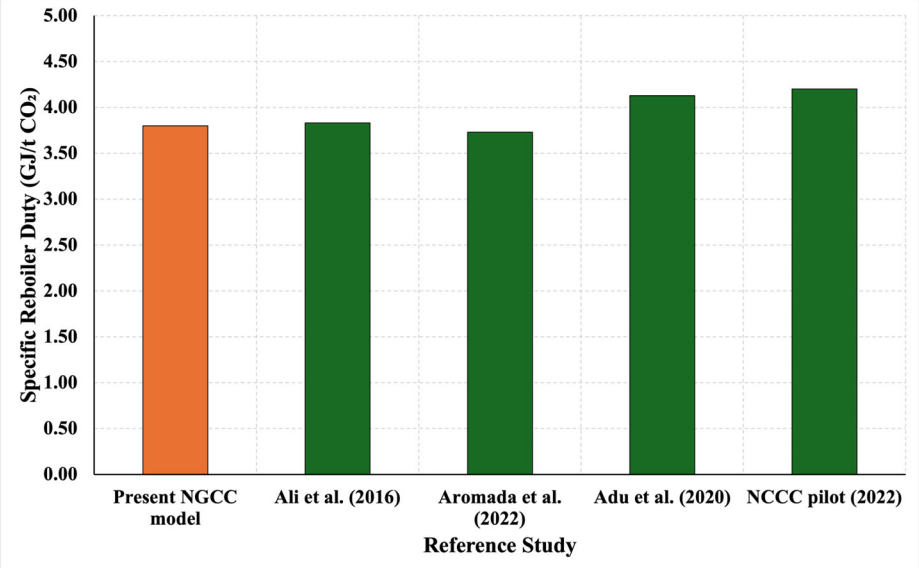


Figure 9. Specific reboiler duty (GJ/t CO_2) for the present NGCC–MEA case and published simulation and NCCC pilot references. Operating conditions differ among studies [1,30,35,36].

3.3.2. Mass-Balance Consistency and Comparison with an NGCC–MEA Reference Case

To complement the quantitative regeneration-energy benchmarking in Section 3.3.1, a steady-state solvent mass balance was established for the present NGCC–PCC reference case and compared with the NGCC configuration without exhaust-gas recirculation reported by Ali et al. [30]. The corresponding operating parameters and specific reboiler duties are compared in Table 9. The present flue-gas stream contains $\mathbf{69.90}$ kg s^{-1} of CO_2 in a total wet-gas flow of $\mathbf{1106.38}$ kg s^{-1}. At $\mathbf{90}$% capture, the absorbed CO_2 flow is $\mathbf{62.91}$ kg s^{-1}. For the specified lean and rich loadings, the required MEA mass flow is obtained from the steady state CO_2 balance:

$$\dot{m}_{\mathrm{MEA}} = \frac{\dot{m}_{\mathrm{CO_2,cap}}\, M_{\mathrm{MEA}}}{(\alpha_{\mathrm{rich}} - \alpha_{\mathrm{lean}})\, M_{\mathrm{CO_2}}} = \frac{62.91 \times 61.083}{(0.48 - 0.25) \times 44.0095} = 379.635 \text{ kg s}^{-1}.$$

For a $\mathbf{30}$ wt% MEA solution on a CO_2-free MEA/water basis, the corresponding aqueous-solvent circulation and solvent-to-flue-gas mass ratio are

$$\dot{m}_{\mathrm{sol,0}} = \frac{379.635}{0.30} = 1265.45 \text{ kg s}^{-1}, \qquad (L/G)_0 = \frac{1265.45}{1106.38} = 1.144.$$

Table 9. Operating parameters and specific reboiler duty for the present NGCC–PCC reference case and the no-EGR case of Ali et al. [30].

Parameter	Present NGCC–PCC Case	Ali et al. [30], No EGR
Wet flue-gas flow (kg s^{-1})	1106.38	1029.7
Inlet CO_2 (mol%, wet basis)	4.08	3.91
MEA concentration (wt%)	30	30
CO_2 capture (%)	90	90
Lean loading (mol CO_2/mol MEA)	0.25	0.20
Rich loading (mol CO_2/mol MEA)	0.48	0.480
Aqueous-solvent flow (kg s^{-1})	1265.45	988.5 *
Solvent-to-gas mass ratio (kg/kg)	1.144	0.96 *
Specific reboiler duty (GJ/t CO_2)	3.80	3.83

* Reference values correspond to the optimized NGCC–MEA configuration without exhaust-gas recirculation reported by Ali et al. [30].

The reboiler heat-stream value of $\mathbf{239.07}$ MW reported for the present case corresponds to a specific reboiler duty of $\mathbf{3.80}$ GJ/t CO_2 at the captured CO_2 flow of $\mathbf{62.91}$ kg s^{-1}. Its absolute deviation from the published value is

$$\delta_q = \frac{|3.80 - 3.83|}{3.83} \times 100\% = 0.78\%.$$

The calculated circulation requirement satisfies the stated solvent-loading and captured-CO_2 balance. Relative to Ali et al. [30], the present case uses a higher lean loading and a larger flue-gas flow, which contribute to its greater calculated circulation requirement. The $\mathbf{0.78}$% difference in specific reboiler duty supports agreement in the magnitude of regeneration energy with the independent NGCC–MEA reference.

3.4. Plant-Wide Energy and CO_2 Balance Framework

The plant-wide assessment combines fuel combustion, Brayton-cycle power generation, exhaust-heat recovery in the heat recovery steam generator (HRSG), Rankine-cycle generation, and amine-based post-combustion CO_2 capture (PCC). The mass-flow sensitivity analysis in Figure 2 uses an imposed model-stream flow rate of 3000 kg/s, whereas the plant-wide combustion assessment in Table 10 reports fuel and air flow rates of 24.90 and 1081.48 kg/s, respectively. These mass flow rates represent different process-stream

quantities and should not be interpreted as equivalent flow rates. Importantly, the Gas Turbine 1 output of 445.40 MW reported in Figure 2 and the natural-gas fuel consumption of 24.90 kg/s reported in Table 10 correspond to the same validated operating case, ensuring a consistent fuel-input and power-output basis for the plant-wide thermal efficiency calculations. At the 3000 kg/s sensitivity setting, the reported outputs of Gas Turbine 1 (GT1), Gas Turbine 2 (GT2), and the steam turbine are 445.40, 54.43, and 61.38 MW, respectively. For the integrated electrical balance, the GT1 and GT2 figures represent package electrical outputs after the work of their mechanically coupled air compressors. The steam-turbine output and auxiliary electrical loads are accounted for separately. The NGCC cases with and without PCC are compared at the same fuel-energy input and gas-turbine operating conditions. Their plant-wide performance is summarized in Table 10.

Table 10. Matched plant-wide comparison of NGCC operation with and without PCC at a fuel-energy input of 1222.49 MW.

Parameter	Without PCC	With PCC
Fuel-energy input (MW)	1222.49	1222.49
GT1 package electrical output (MW)	445.40	445.40
GT2 package electrical output (MW)	54.43	54.43
Steam-turbine electrical output (MW)	61.38	13.22
Auxiliary electrical consumption (MW)	13.48	47.31
Net electrical output (MW)	547.73	465.74
Net LHV thermal efficiency (%)	44.80	38.10
CO_2 capture fraction (%)	0.00	90.00
CO_2 captured (kg/s)	0.00	62.91
Specific reboiler duty (GJ/t CO_2)	—	3.80
Reboiler thermal duty (MW)	0.00	239.07
Steam extraction for regeneration (kg/s)	0.00	114.09
Steam-turbine power reduction (MW)	0.00	48.16
CO_2-compression electric power (MW)	0.00	24.64
Direct CO_2 emissions intensity (kg/MWh)	459.44	54.03

3.4.1. Fuel, Combustion-Air, and Flue-Gas Mass Balances

The total natural-gas mass flow rate is 24.90 kg/s, and its lower heating value (LHV) is 49.096 MJ/kg, corresponding to a fuel-energy input of 1222.49 MW. The fuel contains methane, ethane, propane, n-butane, and n-pentane at mass fractions of 0.70, 0.20, 0.05, 0.03, and 0.02, respectively. Combustion air contains oxygen and nitrogen at mass fractions of 0.2329 and 0.7671. Fuel-energy input is calculated as

$$\dot{E}_{\mathbf{fuel}} = \dot{m}_{\mathbf{fuel}}\mathbf{LHV} = \mathbf{24.90 \times 49.096 = 1222.49\ MW}.$$

Complete oxidation of a hydrocarbon species is represented by

$$\mathbf{C}_n\mathbf{H}_m + \left(n + \frac{m}{4}\right)\mathbf{O_2} \rightarrow n\mathbf{CO_2} + \frac{m}{2}\mathbf{H_2O}.$$

The fuel-derived CO_2 production and stoichiometric oxygen requirement are calculated from the constituent fuel mass fractions:

$$\dot{m}_{\mathbf{CO_2,formed}} = \dot{m}_{\mathbf{fuel}} \sum_i \left(w_i \frac{n_{\mathrm{C},i} M_{\mathrm{CO_2}}}{M_i}\right) = \mathbf{69.90\ kg\,s^{-1}},$$

$$\dot{m}_{\mathbf{O_2,required}} = \dot{m}_{\mathbf{fuel}} \sum_i \left[w_i \frac{\left(n_{\mathrm{C},i} + n_{\mathrm{H},i}/4\right) M_{\mathrm{O_2}}}{M_i}\right] = \mathbf{97.04\ kg\,s^{-1}},$$

where w_i and M_i are the mass fraction and molecular mass of fuel constituent i, respectively, and $n_{C,i}$ and $n_{H,i}$ denote the corresponding numbers of carbon and hydrogen atoms per molecule. The wet-basis CO_2 mole fraction in the combined combustion products is determined from

$$y_{CO_2,wet} = \frac{\dot{n}_{CO_2}}{\dot{n}_{CO_2} + \dot{n}_{H_2O} + \dot{n}_{O_2,excess} + \dot{n}_{N_2}} = 0.0408.$$

The water formed by combustion and the oxygen and nitrogen remaining in the product stream satisfy

$$\dot{m}_{H_2O} = \dot{m}_{fuel} \sum_i \left(w_i \frac{n_{H,i} M_{H_2O}}{2M_i} \right) = 52.04 \text{ kg s}^{-1},$$

$$\dot{m}_{O_2,excess} = Y_{O_2} \dot{m}_{air} - \dot{m}_{O_2,required} = 154.84 \text{ kg s}^{-1},$$

$$\dot{m}_{N_2} = Y_{N_2} \dot{m}_{air} = 829.60 \text{ kg s}^{-1}.$$

The resulting fresh combustion-air flow is 1081.48 kg/s, with 963.71 kg/s supplied to GT1 and 117.77 kg/s to GT2. The corresponding fuel streams are 22.19 and 2.71 kg/s. The overall air-to-fuel ratio is

$$AFR = \frac{\dot{m}_{air,GT1} + \dot{m}_{air,GT2}}{\dot{m}_{fuel}} = \frac{1081.48}{24.90} = 43.43$$

Under complete combustion, the combined wet flue gas contains 69.90 kg/s CO_2, 52.04 kg/s H_2O, 154.84 kg/s excess O_2, and 829.60 kg/s N_2. The combustion-boundary mass balance is therefore

$$\dot{m}_{flue} = \dot{m}_{air} + \dot{m}_{fuel} = 1081.48 + 24.90 = 1106.38 \text{ kg s}^{-1}.$$

The wet- and dry-basis CO_2 mole fractions are 4.08 and 4.41 mol.%, respectively. For the PCC configuration, 90% recovery yields

$$\dot{m}_{CO_2,captured} = \eta_{capture} \dot{m}_{CO_2,formed} = 0.90 \times 69.90 \approx 62.91 \text{ kg s}^{-1},$$

$$\dot{m}_{CO_2,stack} = \dot{m}_{CO_2,formed} - \dot{m}_{CO_2,captured} = 6.99 \text{ kg s}^{-1}.$$

The wet-gas outlet flow after CO_2 separation is

$$\dot{m}_{gas,treated} = \dot{m}_{flue} - \dot{m}_{CO_2,captured} = 1043.47 \text{ kg s}^{-1}.$$

This external gas-flow balance excludes internal solvent-circulation streams. Table 11 summarizes the stream and species balances for the two configurations.

Table 11. Fuel, combustion-air, flue-gas, and CO_2 stream balances for NGCC operation with and without PCC.

Stream Variable	Without PCC	With PCC
Natural-gas fuel to GT1 (kg/s)	22.19	22.19
Natural-gas fuel to GT2 (kg/s)	2.71	2.71
Total natural-gas fuel (kg/s)	24.90	24.90
Fresh air to GT1 (kg/s)	963.71	963.71
Fresh air to GT2 (kg/s)	117.77	117.77
Total fresh combustion air (kg/s)	1081.48	1081.48
Overall air-to-fuel mass ratio (kg/kg)	43.43	43.43
O_2 consumed by combustion (kg/s)	97.04	97.04
Unconsumed O_2 in wet flue gas (kg/s)	154.84	154.84
N_2 in wet flue gas (kg/s)	829.60	829.60
H_2O in wet flue gas (kg/s)	52.04	52.04

https://doi.org/10.3390/en19225541

CO_2 generated (kg/s)	69.90	69.90
Total wet-flue-gas flow (kg/s)	1106.38	1106.38
CO_2 mole fraction, wet basis (mol.%)	4.08	4.08
CO_2 mole fraction, dry basis (mol.%)	4.41	4.41
CO_2 captured (kg/s)	0.00	62.91
CO_2 discharged to stack (kg/s)	69.90	6.99
Wet gas discharged to stack (kg/s)	1106.38	1043.47

3.4.2. Gas-Turbine, Steam-Cycle, and CO_2-Capture Energy Balances

The gas-turbine calculations use a compressor-inlet temperature of 298.15 K, compressor isentropic efficiency of 0.86, turbine isentropic efficiency of 0.9063, combustion efficiency of 0.995, and generator efficiency of 0.992. Representative heat capacities of 1.005 and 1.16 kJ kg^{-1} K^{-1} are used for air and the combustion products, respectively. Compressor and expansion work are evaluated as

$$\boldsymbol{w_c = \frac{c_{p,a} T_1}{\eta_c}\left[r_p^{(\gamma_a - 1)/\gamma_a} - 1\right]},$$

$$\boldsymbol{w_t = \eta_t c_{p,g} T_3 \left[1 - r_p^{-(\gamma_g - 1)/\gamma_g}\right]},$$

where $\boldsymbol{w_c}$ and $\boldsymbol{w_t}$ are expressed in kJ/kg, $\boldsymbol{r_p}$ is compressor pressure ratio, and $\boldsymbol{\gamma}$ is the ratio of specific heats. The combustor energy equation, with all terms expressed in MW on the same sensible-enthalpy basis, is

$$\boldsymbol{\frac{\dot{m}_{flue} c_{p,g}(T_3 - T_1)}{1000} = \frac{\dot{m}_{air} w_c}{1000} + \eta_b \dot{m}_{fuel} LHV}.$$

Because compressor work is already included within each gas-turbine package, the package electrical output is

$$\boldsymbol{P_{GT,package} = \frac{\eta_{gen}}{1000}(\dot{m}_{flue} w_t - \dot{m}_{air} w_c)}.$$

The model yielded a compressor pressure ratio of 20.02, compressor outlet temperature of 494.08 °C, combustor/turbine inlet temperature of 1370.04 °C, and turbine exhaust temperature of 580.18 °C. The calculated gross turbine shaft power was 1013.70 MW, and the mechanically coupled compressor shaft consumption was 509.84 MW. With generator losses accounted for, the combined package output was 499.83 MW, matching the GT1 and GT2 outputs of 445.40 and 54.43 MW reported in Figure 2. Compressor consumption is therefore not deducted again in calculating net plant power.

The steam cycle generated 61.38 MW without capture from a steam mass flow of 120.50 kg/s, an effective turbine enthalpy drop of 514.52 kJ/kg, and an electrical efficiency of 0.99:

$$\boldsymbol{P_{ST,without\ PCC} = \frac{\eta_{ST,g} \dot{m}_{steam} \Delta h_{ST}}{1000} = 61.38\ MW}.$$

With an HRSG-side steam enthalpy rise of 2550 kJ/kg, the heat delivered to the steam system and the exhaust energy available for recovery are

$$\boldsymbol{\dot{Q}_{HRSG} = \frac{\dot{m}_{steam} \Delta h_{HRSG}}{1000} = 307.28\ MW},$$

$$\boldsymbol{\dot{Q}_{exhaust} = \frac{\dot{m}_{flue} c_{p,g}(T_4 - T_1)}{1000} = 712.52\ MW}.$$

Because HRSG heat absorption is below the exhaust sensible energy available for recovery, the corresponding calculated HRSG gas-outlet temperature was 340.76 °C.

The amine-regeneration requirement is calculated from the specific reboiler duty and the captured CO_2 mass flow rate:

$$\dot{Q}_{\mathrm{reb}} = q_{\mathrm{reb}}\dot{m}_{\mathrm{CO_2,captured}} = 3.80 \times 62.91 = 239.07\ \mathrm{MW},$$

where $q_{\mathrm{reb}} = 3.80\ \mathrm{GJ\,t_{CO_2}^{-1}}$ (numerically equal to 3.80 MJ/kg CO_2). This specific duty is obtained directly from the HYSYS reboiler heat stream under the solvent and column settings of Section 2.3. Using a useful steam condensation enthalpy change of 2095.37 kJ/kg, the extraction mass flow rate was

$$\dot{m}_{\mathrm{steam,extracted}} = \frac{1000\dot{Q}_{\mathrm{reb}}}{\Delta h_{\mathrm{reb}}} = 114.09\ \mathrm{kg\,s^{-1}}.$$

This extraction rate is lower than the total steam flow of 120.50 kg/s. The extracted steam no longer undergoes the downstream turbine expansion, for which the effective enthalpy drop is 426.37 kJ/kg. The resulting electrical penalty and remaining steam-turbine power are

$$\Delta P_{\mathrm{ST}} = \frac{\eta_{\mathrm{ST,g}}\dot{m}_{\mathrm{steam,extracted}}\Delta h_{\mathrm{LP}}}{1000} = 48.16\ \mathrm{MW},$$

$$P_{\mathrm{ST,with\ PCC}} = P_{\mathrm{ST,without\ PCC}} - \Delta P_{\mathrm{ST}} = 13.22\ \mathrm{MW}.$$

The electrical requirement of CO_2 compression was 24.64 MW, evaluated using a compression-inlet temperature of 311.45 K, inlet and outlet pressures of 1.21 and 119.45 bar, an isothermal efficiency of 0.69, and a CO_2-specific gas constant of 0.1889 kJ kg^{-1} K^{-1}:

$$P_{\mathrm{CO_2,comp}} = \frac{\dot{m}_{\mathrm{CO_2,captured}}R_{\mathrm{CO_2}}T_{\mathrm{comp}}}{1000\eta_{\mathrm{isoth}}}\ln\left(\frac{p_{\mathrm{out}}}{p_{\mathrm{in}}}\right) = 24.64\ \mathrm{MW}.$$

The electrical auxiliaries consumed 13.48 MW. With PCC, the auxiliary total of 47.31 MW includes these existing loads plus 24.64 MW for CO_2 compression, 3.29 MW for solvent pumps, 4.16 MW for the flue-gas booster fan, and 1.74 MW for additional cooling and handling. Net power and net fuel-based thermal efficiency are obtained as

$$P_{\mathrm{net}} = P_{\mathrm{GT1,package}} + P_{\mathrm{GT2,package}} + P_{\mathrm{ST}} - P_{\mathrm{aux}},$$

$$\eta_{\mathrm{net,LHV}} = \frac{P_{\mathrm{net}}}{\dot{m}_{\mathrm{fuel}}\mathrm{LHV}} \times 100\%.$$

Net electrical output decreased from 547.73 MW without PCC to 465.74 MW with PCC. The corresponding net LHV efficiencies were 44.80% and 38.10%, respectively. The efficiency penalty calculated from unrounded values was 6.71 percentage points. Direct CO_2 emissions intensity was calculated as

$$I_{\mathrm{CO_2}} = \frac{3600\dot{m}_{\mathrm{CO_2,stack}}}{P_{\mathrm{net}}}, \qquad \left[I_{\mathrm{CO_2}}\right] = \mathrm{kg\,MWh^{-1}}.$$

The calculated direct CO_2 emissions intensity decreased from 459.44 to 54.03 kg CO_2/MWh. Reboiler duty represents internal heat transfer from the steam cycle to the solvent. It was not subtracted separately from the net electrical output because its electrical effect was already included in the steam-turbine output reduction.

3.4.3. Overall Mass, Carbon, and Energy-Balance Closure

The integrated system boundaries include all incoming combustion-air and fuel streams, outgoing stack and captured-CO_2 streams, net exported electrical work, and external heat rejection. The internal solvent recirculation and reboiler heat transfer do not cross the overall system boundary. All energy terms are evaluated relative to a consistent

thermodynamic datum. The overall mass-balance, carbon/CO_2-balance, and energy-balance residuals are calculated as

$$R_{\mathrm{m}} = \frac{|\sum \dot{m}_{\mathrm{in}} - \sum \dot{m}_{\mathrm{out}}|}{\sum \dot{m}_{\mathrm{in}}} \times 100\%,$$

$$R_{\mathrm{CO_2}} = \frac{|\dot{m}_{\mathrm{CO_2,formed}} - \dot{m}_{\mathrm{CO_2,captured}} - \dot{m}_{\mathrm{CO_2,stack}}|}{\dot{m}_{\mathrm{CO_2,formed}}} \times 100\%,$$

$$R_{\mathrm{E}} = \frac{|\dot{E}_{\mathrm{in}} - \dot{E}_{\mathrm{out}}|}{\dot{E}_{\mathrm{in}}} \times 100\%.$$

The accepted maximum residuals are 0.10% for overall mass conservation, 0.50% for energy conservation, and 0.10% for the carbon/CO_2 balance. In the whole-plant energy ledger, the fuel input is allocated among exported electricity, the sensible energy of outgoing gas and CO_2 product streams, and heat rejected to the external surroundings:

$$\dot{E}_{\mathrm{fuel}} = P_{\mathrm{net}} + \dot{Q}_{\mathrm{stack}} + \dot{Q}_{\mathrm{CO_2,product}} + \dot{Q}_{\mathrm{rejected}}.$$

The sensible energy of the outgoing material streams is evaluated relative to the ambient temperature datum, while external heat rejection accounts for the remaining external heat transfers:

$$\dot{Q}_{\mathrm{stack}} = \frac{\dot{m}_{\mathrm{stack}} c_{p,\mathrm{stack}} (T_{\mathrm{stack}} - T_{\mathrm{datum}})}{1000},$$

$$\dot{Q}_{\mathrm{rejected}} = \dot{E}_{\mathrm{fuel}} - P_{\mathrm{net}} - \dot{Q}_{\mathrm{stack}} - \dot{Q}_{\mathrm{CO_2,product}}.$$

Without PCC, outgoing energy comprised 547.73 MW of net electricity, 405.24 MW of stack sensible energy, and 268.55 MW of heat rejection. With PCC, the corresponding contributions were 465.74 MW of net electricity, 21.52 MW of treated-gas sensible energy, 0.80 MW of captured-CO_2 sensible energy, and 732.28 MW of heat rejection. Energy-balance residuals were 0.08% and 0.18%, respectively. Both were below the 0.50% acceptance limit. Table 12 summarizes the mass, carbon/CO_2, and energy balances and their closure residuals.

Table 12. Overall mass, carbon/CO_2, and energy balances for NGCC operation with and without PCC.

Balance Variable	Without PCC	With PCC	Acceptance Limit (%)
Total external mass entering (kg/s)	1106.38	1106.38	—
Total external mass leaving (kg/s)	1106.14	1106.17	—
Overall mass-balance residual (%)	0.02	0.02	≤0.10
CO_2 formed by combustion (kg/s)	69.90	69.90	—
CO_2 collected in capture product (kg/s)	0.00	62.89	—
CO_2 discharged to stack (kg/s)	69.88	6.98	—
Carbon/CO_2-balance residual (%)	0.03	0.04	≤0.10
External fuel-energy input (MW)	1222.49	1222.49	—
Net exported electricity (MW)	547.73	465.74	—
Stack-gas sensible energy (MW)	405.24	21.52	—
Captured CO_2-product sensible energy (MW)	0.00	0.80	—
Heat rejected to surroundings (MW)	268.55	732.28	—
Total external energy leaving (MW)	1221.52	1220.34	—
Overall energy-balance residual (%)	0.08	0.18	≤0.50

For the without-PCC and with-PCC configurations, respectively, the overall mass residuals are 0.02% and 0.02%, the carbon/CO_2 residuals are 0.03% and 0.04%, and the energy residuals are 0.08% and 0.18%.

4. Limitations and Future Work

This study combined component-level numerical sensitivity diagnostics with a matched plant-wide comparison of NGCC operation with and without PCC. The plant-wide analysis quantified energy and CO_2 balances at the reference conditions. The separate sweeps did not establish net plant performance across their full ranges. Their different fixed references prevent ranking of output magnitudes or slopes across sweeps.

The one-variable-at-a-time approach does not quantify input interactions. It cannot identify an optimum that accounts for compressor and turbine limits, solvent stability, and HRSG heat-transfer constraints.

The first-law assessment in Analytical Energy Assessment of the Temperature Sensitivity (Section 3.2) estimated sensible-heating requirements using a constant air-equivalent specific heat. A more complete evaluation would use composition-dependent enthalpy and specify the heating source. It would also account for changes in fuel consumption, compressor work, and auxiliary loads. The high-temperature diagnostic results remain conditional on the imposed heating boundary and cannot be extrapolated to practical compressor-inlet conditions. Sweeps around a common, physically feasible reference would permit direct comparison of net electrical output and thermal efficiency.

The simulated specific reboiler duty of 3.80 GJ/t CO_2 differed from the three NGCC–MEA simulation references by 0.78–7.99%. The MAPD was 3.55%. The difference relative to the independent NCCC pilot result was approximately 9.52%. These comparisons used studies with different operating conditions and capture-system configurations.

Validation under matched conditions is still needed for CO_2 removal, solvent loadings, and reboiler duty. Such validation could use mean absolute percentage error and root mean square error where suitable reference data are available. Future work should also examine constrained multivariable optimization, exergy, electricity generation costs, and CO_2 avoidance costs.

5. Conclusions

An Aspen HYSYS model was developed for an NGCC plant integrated with amine-based PCC. Component-level numerical diagnostics examined model-stream temperature, pressure, and mass flow. Separate scans examined solvent circulation, absorber conditions, and regeneration parameters.

The three power-cycle sweeps used different fixed references, so their output magnitudes and slopes cannot be ranked across sweeps. Increasing imposed stream temperature from 100 to 500 °C raised combined turbine output by 29.60 MW. The estimated additional sensible-heating requirement was 1206.0 MW. This response was conditional on the imposed heating boundary and did not establish a practical compressor-inlet heating benefit or improved net plant efficiency.

The matched plant-wide assessment quantified the energy and emissions effects of PCC integration. Net electrical output decreased from 547.73 to 465.74 MW. Net thermal efficiency decreased from 44.80% to 38.10%, with an approximately 6.71-percentage-point penalty calculated from unrounded values.

At 90% CO_2 capture, the simulated specific reboiler duty was 3.80 GJ/t CO_2. Direct CO_2 emissions intensity decreased from 459.44 to 54.03 kg CO_2/MWh. The specific reboiler duty was within the published NGCC–MEA simulation range of 3.73–4.13 GJ/t CO_2. The

MAPD across the three simulation references was 3.55%; the independent NCCC comparison was assessed separately.

The results quantified the trade-off between lower direct CO_2 emissions and the steam-cycle and auxiliary-power requirements of PCC. Further work should extend the plant-wide analysis across common reference conditions and validate capture predictions against matched independent data. Multivariable optimization, exergy analysis, and techno-economic evaluation would support assessment of practical feasibility.

Author Contributions: A.R.: Conceptualization, methodology, software, formal analysis, investigation, writing—original draft. H.K.: Visualization, methodology, formal analysis, data curation. A.U.Y.: Conceptualization, validation, data curation. M.A.R.: Methodology, writing—review and editing. A.I.: Formal Analysis—review and editing. M.A.: Investigation and validation. M.Z.F.: Methodology, formal analysis, software, investigation, resources, and validation. S.u.d.: Resources, visualization, and writing—review and editing. All authors have read and agreed to the published version of the manuscript.

Funding: This research received no external funding.

Data Availability Statement: The data supporting the reported results are available in the manuscript.

Acknowledgments: During the preparation of this manuscript, the authors used ChatGPT (OpenAI) v6 to assist with manuscript drafting, language refinement, and text organization. The authors reviewed and edited the AI-assisted content and take full responsibility for the accuracy, originality, and integrity of the published work.

Conflicts of Interest: The authors declare no conflicts of interest.

References

1. Adu, E.; Zhang, Y.D.; Liu, D.; Tontiwachwuthikul, P. Parametric process design and economic analysis of post-combustion CO_2 capture and compression for coal- and natural gas-fired power plants. *Energies* **2020**, *13*, 2519. https://doi.org/10.3390/en13102519.
2. Fu, S.; Tang, X.; Rehan, M.A.; Li, G. A thermodynamic study and numerical analysis of Ericsson, Brayton, and Carnot cycles for the thermally regenerative electrochemical refrigerator. *Energy Convers. Manag.* **2025**, *325*, 119422. https://doi.org/10.1016/j.enconman.2024.119422.
3. Loni, R.; Najafi, G.; Bellos, E.; Rajaee, F.; Said, Z.; Mazlan, M. A review of industrial waste heat recovery system for power generation with Organic Rankine Cycle: Recent challenges and future outlook. *J. Clean. Prod.* **2021**, *287*, 125070. https://doi.org/10.1016/j.jclepro.2020.125070.
4. Rehan, M.A. Solar Photothermal CO_2 Conversion: Harnessing Light and Heat for Carbon Neutrality: A Mini Review. *J. Clim. Chang.* **2026**, *12*, 16. https://doi.org/10.70917/jcc-2026-013.
5. Isogai, H.; Nakagaki, T. Exploration of optimal operating conditions for a natural gas combined-cycle power plant integrated with post-combustion CO_2 capture using 2-amino-2-methyl-1-propanol/piperazine considering the propagation effect. *Int. J. Greenh. Gas Control* **2023**, *122*, 103816. https://doi.org/10.1016/j.ijggc.2022.103816.
6. Al-Elanjawy, Y.A.H.; Yilmaz, M. Solar-Assisted Carbon Capture Process Integrated with a Natural Gas Combined Cycle (NGCC) Power Plant—A Simulation-Based Study. *Processes* **2024**, *12*, 613. https://doi.org/10.3390/pr12030613.
7. Akbari, M.; Khalilarya, S. Emergy and stability analysis of a biomass-fueled combined cycle integrating Rankine and Brayton cycles with desalination and CO_2 recycling. *Int. J. Hydrogen Energy* **2026**, *203*, 153185. https://doi.org/10.1016/j.ijhydene.2025.153185.
8. Yadav, S.; Seethamraju, S.; Banerjee, R. Post-combustion CO_2 capture using cold energy from liquefied natural gas regasification in natural gas combined cycle power plants. *Fuel* **2025**, *401*, 135878. https://doi.org/10.1016/j.fuel.2025.135878.
9. Dai, T.; Xu, C.; Li, S.; Shao, M.; Ma, Y.; Xin, T. Thermodynamic analysis and operation strategy optimization of a coal-fired power plant incorporating the CO_2 capture process. *Energy* **2025**, *335*, 138349. https://doi.org/10.1016/j.energy.2025.138349.

10. Canepa, R.; Wang, M.; Biliyok, C.; Satta, A. Thermodynamic analysis of combined cycle gas turbine power plant with post-combustion CO_2 capture and exhaust gas recirculation. *Proc. Inst. Mech. Eng. Part E J. Process Mech. Eng.* **2013**, *227*, 89–105. https://doi.org/10.1177/0954408912469165.
11. Gu, F.; Zhu, Z.; Shi, Q.; Li, R. Thermodynamic and economic analyses of natural gas combined cycle power plants with and without the presence of organic Rankine cycle. *Energy Explor. Exploit.* **2023**, *41*, 1956–1982. https://doi.org/10.1177/01445987231183178.
12. Biliyok, C.; Yeung, H. Evaluation of natural gas combined cycle power plant for post-combustion CO_2 capture integration. *Int. J. Greenh. Gas Control* **2013**, *19*, 396–405. https://doi.org/10.1016/j.ijggc.2013.10.003.
13. Petrovic, A.B.; Soltani, M. Optimization of post combustion CO_2 capture from a combined-cycle gas turbine power plant via Taguchi design of experiment. *Processes* **2019**, *7*, 364. https://doi.org/10.3390/pr7060364.
14. Baghsheikhi, M.; Shafiei, P.; Mohammadi, M. Energy, Exergy, and Exergoeconomic Analysis of a Combined Cycle Power Plant with Post-Combustion CO_2 Capture: A Case Study in Northern Iran. *Energy Sci. Eng.* **2025**, *13*, 5075–5092. https://doi.org/10.1002/ese3.70230.
15. Ahn, J.H.; Jeong, J.H.; Choi, B.S.; Kim, T.S. Influence of various carbon capture technologies on the performance of natural gas-fired combined cycle power plants. *J. Mech. Sci. Technol.* **2019**, *33*, 1431–1440. https://doi.org/10.1007/s12206-019-0245-x.
16. Hu, Y.; Xu, G.; Xu, C.; Yang, Y. Thermodynamic analysis and techno-economic evaluation of an integrated natural gas combined cycle (NGCC) power plant with post-combustion CO_2 capture. *Appl. Therm. Eng.* **2017**, *111*, 308–316. https://doi.org/10.1016/j.applthermaleng.2016.09.094.
17. Esquivel-Patiño, G.G.; Nápoles-Rivera, F.; Jiménez-Gutiérrez, A. Thermal integration of a natural gas combined cycle power plant with carbon capture and utilization technologies. *Energy Convers. Manag.* **2023**, *295*, 117619. https://doi.org/10.1016/j.enconman.2023.117619.
18. Li, Y.; Zhu, R.; Huang, B.; Huang, W. Towards the minimum equivalent carbon emission of soil thermal desorption remediation by post-combustion carbon capture. *J. Environ. Manag.* **2026**, *401*, 129012. https://doi.org/10.1016/j.jenvman.2026.129012.
19. Zhuang, H.; Zhang, Y.; Takyi, S.A.; Lv, J.; Lei, Z.; Xin, Y.; Tontiwachwuthikul, P. Pilot-scale investigation and simulation-based optimization of MDEA/PZ for post-combustion CO_2 capture. *Energy* **2026**, *347*, 140387. https://doi.org/10.1016/j.energy.2026.140387.
20. Esfandyari, M.; Moghaddam, A.H. Comparative analysis of amine-based solvents for energy efficient post-combustion CO_2 capture. *Fuel* **2025**, *402*, 135982. https://doi.org/10.1016/j.fuel.2025.135982.
21. Adu, E.; Li, Y.; Zhang, Y.; Xin, Y.; Tontiwachwuthikul, P. Optimization and energy assessment of technological process for CO_2 capture system of natural gas and coal combustion. *Energy Rep.* **2022**, *8*, 7612–7627. https://doi.org/10.1016/j.egyr.2022.06.004.
22. Li, Y.; Wang, N.; Guan, H.; Jia, Z.; Zhang, Y.; Zhao, G.; Gao, M. Optimization study of CO_2 capture unit for subcritical coal-fired power generation unit based on Ebsilon and Aspen Plus. *Energy Convers. Manag.* **2022**, *269*, 116111. https://doi.org/10.1016/j.enconman.2022.116111.
23. Khan, H.; Tariq, R.; Shah, S.N.; Shahzad, M.W.; Ahmad, T.; Sheikh, N.A. Thermodynamic and technoeconomic comparative justification of a waste heat recovery process with integration of multifluid and indirect evaporative cooler. *Int. Commun. Heat Mass Transf.* **2022**, *139*, 106416. https://doi.org/10.1016/j.icheatmasstransfer.2022.106416.
24. Luo, X.; Wang, M.; Chen, J. Heat integration of natural gas combined cycle power plant integrated with post-combustion CO_2 capture and compression. *Fuel* **2015**, *151*, 110–117. https://doi.org/10.1016/j.fuel.2015.01.030.
25. Kopac, T.; Demirel, Y. Impact of thermodynamics and kinetics on the carbon capture performance of the amine-based CO_2 capture system. *Environ. Sci. Pollut. Res. Int.* **2024**, *31*, 39350–39371. https://doi.org/10.1007/s11356-024-33792-y.
26. Haque, M.E.; Summits, S.; Giridhar, N.V.; Ijiyinka, I.S.; Le, Q.M.; Zhang, Z.; Mobley, P.; Gupta, V.; Jiang, Y.; Freeman, C.J.; et al. Net Present Value Optimization of a Natural Gas Combined Cycle Plant with CO_2 Capture using a Water-Lean Solvent Considering Transient Electricity Price for Multiple Regions. *Ind. Eng. Chem. Res.* **2025**, *64*, 22790–22812. https://doi.org/10.1021/acs.iecr.5c02872.
27. Entezari, A.; Saifoddin, A.; Aslani, A.; Yousefi, H. Optimizing combined cycle and integrated ORC waste heat recovery for enhanced energy efficiency in aqueous post-combustion carbon capture. *Energy Convers. Manag.* **2026**, *348*, 120755. https://doi.org/10.1016/j.enconman.2025.120755.
28. Gaitán-Vélez, V.; Esquivel-Patiño, G.G.; Jiménez-Gutiérrez, A. Environmental and economic analysis of a natural gas combined cycle power plant using CO_2 utilization technologies and ecosystem services. *ACS Sustain. Chem. Eng.* **2023**, *11*, 7218–7230. https://doi.org/10.1021/acssuschemeng.3c01122.

29. Ayyad, A.; Abbas, A.; Elminshawy, N. A simulation study of the effect of post-combustion amine-based carbon-capturing integrated with solar thermal collectors for combined cycle gas power plant. *Discov. Sustain.* **2021**, *2*, 9. https://doi.org/10.1007/s43621-021-00018-x.
30. Ali, U.; Agbonghae, E.O.; Hughes, K.J.; Ingham, D.B.; Ma, L.; Pourkashanian, M. Techno-economic process design of a commercial-scale amine-based CO_2 capture system for natural gas combined cycle power plant with exhaust gas recirculation. *Appl. Therm. Eng.* **2016**, *103*, 747–758. https://doi.org/10.1016/j.applthermaleng.2016.04.145.
31. Liang, Y.; Lei, T.; Zhu, Y.; Ye, K.; Wu, J.; Dong, M.; Lu, J. Energy consumption optimization of CO_2 capture and compression in natural gas combined cycle power plant through configuration modification and process integration. *Appl. Therm. Eng.* **2024**, *255*, 124019. https://doi.org/10.1016/j.applthermaleng.2024.124019.
32. Amrollahi, Z.; Ertesvåg, I.S.; Bolland, O. Thermodynamic analysis on post-combustion CO_2 capture of a natural-gas-fired power plant. *Int. J. Greenh. Gas Control* **2011**, *5*, 422–426. https://doi.org/10.1016/j.ijggc.2010.09.004.
33. Cheng, P.; Jia, L.; Zhao, J.-H.; Wu, Y.-W.; Yu, Y.; Gao, X.-F.; Meng, Q.; Jin, Y. Study on the mechanism of synergistic adsorption of CO_2 and Hg^0 by Mg-MOF-74-derived modified composites based on experiment and density functional theory. *Chem. Eng. J.* **2026**, *544*, 179203. https://doi.org/10.1016/j.cej.2026.179203.
34. Rehman, A.; Hussain, A.; Iqbal, M.M.; Khan, H.; Usman, A. Optimization and Performance Analysis of Natural Gas-Based Combined Cycle Power Plant Using Post Combustion Process. In Proceedings of the 12th International Mechanical Engineering Conference (IMEC 2023), Karachi, Pakistan, 10–11 May 2023; pp. 138–147.
35. Aromada, S.A.; Eldrup, N.H.; Øi, L.E. Cost and Emissions Reduction in CO_2 Capture Plant Dependent on Heat Exchanger Type and Different Process Configurations: Optimum Temperature Approach Analysis. *Energies* **2022**, *15*, 425. https://doi.org/10.3390/en15020425.
36. Zhou, S.J.; Rayer Rabindran, A.V.; Gupta, R. *Ionic Liquid Catalyzed MEA Solvent for Post-Combustion CO_2 Capture Testing Using the PSTU at NCCC*; Technical Report; Susteon Inc.: Cary, NC, USA, 2022. Available online: https://www.nationalcarboncapturecenter.com/wp-content/uploads/2023/04/Susteon-Final-Report-NCCC-Campaign_opt.pdf (accessed on 2 November 2026).

Disclaimer/Publisher's Note: The statements, opinions and data contained in all publications are solely those of the individual author(s) and contributor(s) and not of MDPI and/or the editor(s). MDPI and/or the editor(s) disclaim responsibility for any injury to people or property resulting from any ideas, methods, instructions or products referred to in the content.